

Flavour anomalies from a split dark sector

Luc Darmé,^a Marco Fedele,^b Kamila Kowalska^c and Enrico Maria Sessolo^c

^a *INFN, Laboratori Nazionali di Frascati,
C.P. 13, 100044 Frascati, Italy*

^b *Dept. de Física Quàntica i Astrofísica, Institut de Ciències del Cosmos (ICCUB),
Universitat de Barcelona, Martí i Franquès 1, E-08028 Barcelona, Spain*

^c *National Centre for Nuclear Research,
ul. Pasteura 7, 02-093 Warsaw, Poland*

E-mail: luc.darme@lnf.infn.it, marco.fedele@icc.ub.edu,
kamila.kowalska@ncbj.gov.pl, enrico.sessolo@ncbj.gov.pl

ABSTRACT: We investigate solutions to the flavour anomalies in B decays based on loop diagrams of a “split” dark sector characterised by the simultaneous presence of heavy particles at the TeV scale and light particles around and below the B -meson mass scale. We show that viable parameter space exists for solutions based on penguin diagrams with a vector mediator, while minimal constructions relying on box diagrams are in strong tension with the constraints from the LHC, LEP, and the anomalous magnetic moment of the muon. In particular, we highlight a regime where the mediator lies close to the B -meson mass, naturally realising a resonance structure and a q^2 -dependent effective coupling. We perform a full fit to the relevant flavour observables and analyse the constraints from intensity frontier experiments. Besides new measurements of the anomalous magnetic moment of the muon, we find that decays of the B meson, B_s -mixing, missing energy searches at Belle-II, and LHC searches for top/bottom partners can robustly test these scenarios in the near future.

Contents

1	Introduction	1
2	Effective one-loop Wilson coefficients from split dark sector models	3
2.1	Box diagrams	3
2.2	Penguin diagrams	5
3	Constraints on the model	9
3.1	Flavour constraints	9
3.2	Precision physics constraints	13
4	Fitting procedure and results	15
5	Conclusions	21
A	Appendix: Invisible decay limits	23

1 Introduction

Several flavour anomalies have been observed in the last few years in various B -meson decay measurements by different experimental collaborations. Some of the anomalous measurements involve semileptonic $b \rightarrow s$ transitions and include: (1) the suppression with respect to the Standard Model (SM) expectation of the ratios R_K and R_{K^*} – the branching ratios of the B -meson decay into a K or K^* meson and muons, over the decay to the same kaon and electrons – which were observed at LHCb [1–4] and which imply the possible violation of lepton-flavour universality (LFUV); (2) an enhancement in the angular observable P'_5 , first measured by the LHCb [5] and Belle collaborations [6], and later observed also by ATLAS and CMS [7, 8]; and (3) a suppression in the branching ratios for the decays $B_s \rightarrow \phi \mu^+ \mu^-$ [9] and $B \rightarrow K^{(*)} \mu^+ \mu^-$ [10, 11].

Global effective field theory analyses of the $b \rightarrow s$ data have pointed strongly towards New Physics (NP) in the four-fermion operators $\mathcal{O}_9^{(\prime)\mu}$, $\mathcal{O}_{10}^{(\prime)\mu}$ [12–31]. Different combinations of the corresponding Wilson coefficients seem to be equally favoured, as long as C_9^μ remains significantly below zero. For instance, in a single operator scenario involving only \mathcal{O}_9^μ , a solution consistent with the full set of $b \rightarrow s$ measurements requires approximately $C_9^\mu \in [-1.2, -0.6]$ at the 2σ level.

While the most natural assumption is that heavy states above the scale of electroweak symmetry breaking (EWSB) are responsible for generating these operators, alternative possibilities have emerged in the literature [18, 32–36], that these NP effects are in fact due to the presence of light degrees of freedom around or below the typical scale probed by the experiment.

The solutions based on a light dark sector can be divided roughly into two categories, depending on whether the masses involved lie above or below the characteristic window for LFUV observables, which is commonly identified as ranging roughly from the dimuon threshold to $\sqrt{6} - \sqrt{8}$ GeV. The first category involves a new light vector with mass $m_V \gtrsim 2$ GeV, coupled to the $b - s$ and the muon currents, interfering negatively with the SM amplitude [18, 33]. The light particle can contribute strongly to the physical observables thanks to the proximity of a resonance to the experimental bins [33] and NP effects can be parametrised in this case by Wilson coefficients with an explicit q^2 dependence. Interestingly, the corresponding resonance in the dimuon spectrum from B -meson decay could be hidden due to the sizeable hadronic uncertainty and the presence of the J/Ψ resonance in the same region [33, 37].

A second class of models, featuring instead the exchange of light particles below the dimuon threshold, have been considered in refs. [18, 32, 34, 35]. These scenarios are strongly constrained by a number of observations. On the one hand, a light scalar particle with effective couplings to the s and b quarks and leptons yields a positive contribution to the decay rate. One thus requires a sizeable coupling to electrons, a scenario that is in most cases [34] in tension with the measurement of $B \rightarrow K^{(*)}e^+e^-$ processes in agreement with the SM [38]. On the other hand, a light vector boson with effective couplings to the s and b quark and muons can interfere negatively with the SM process, but is strongly constrained by the measurement of the anomalous magnetic moment $(g - 2)_\mu$. This in turn implies a sizeable coupling to the b and s quarks, leading to strong bounds from B_s mixing. Finally, in ref. [35] it was pointed out that a resonance coupling to electrons can actually be used to reproduce the low- q^2 bin of R_{K^*} . A vector boson very close – but below – the dimuon threshold, where $\mathcal{BR}(B \rightarrow K^{(*)}V)$ can be as small as 1×10^{-7} , can explain the anomaly and escape the limits from ref. [38].

A common trait of the constructions mentioned above is the presence of an effective off-diagonal coupling g_{bs} to the quark current. Since the quarks carry $SU(3)_c$ charge, g_{bs} must arise from particles with colour integrated out in the UV theory, which must be heavy to avoid exclusion by the strong limits from the LHC. This also means that in realistic scenarios g_{bs} will be suppressed by either loop effects, a small tree-level mixing angle between the SM quarks and heavy vector-like (VL) particles, or a combination of both.

In this paper we perform a detailed exploration of the first of these possibilities, i.e, the UV-complete model gives rise to the effective $b - s$ coupling of the light particle via loop effects. We will show that, under these assumptions, in order to generate a g_{bs} large enough to fit the flavour anomalies and, at the same time, maintain reasonable agreement with perturbativity of the couplings, several phenomenological challenges must be faced. In the specific of the cases mentioned above, we will show that solutions with $m_V \gtrsim 2$ GeV can be made viable with appropriate UV completions, even though they are subject to a combination of increasingly tightening bounds that include, in the UV, LHC direct constraints on hadronic and leptonic new states and Drell-Yan dimuon constraints from the Z lineshape, and in the IR, an appropriate width- and bin-dependent treatment of the bounds from $\mathcal{BR}(B \rightarrow K + \text{invisible})$ and $\mathcal{BR}(B \rightarrow K\mu\mu)$. Conversely, the second class of

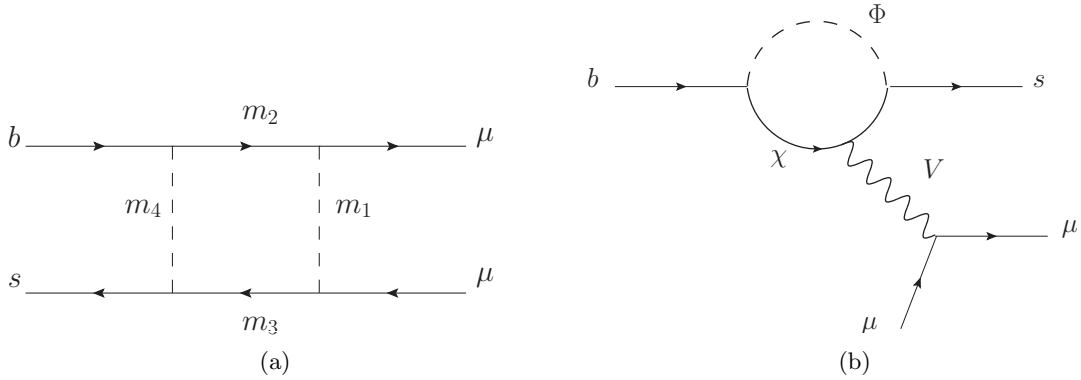


Figure 1: (a) Example box loop mediating the B -meson decay. (b) Example penguin loop mediating the B -meson decay.

solutions, characterised by m_V under the dimuon threshold, is less appealing, as is strongly constrained by a combination of bounds from $\mathcal{BR}(B \rightarrow K + \text{invisible})$, neutrino trident production, intensity frontier limits on kinetic mixing, and $\mathcal{BR}(B_s \rightarrow \mu\mu)$.

More in general, we perform in this work a detailed Monte Carlo scan of the broad m_V range and the loop-induced couplings. We identify and characterise the specific properties of the viable models and provide an indication of possible strategies for a timely detection of the associated NP states.

The paper is organised as follows. In Sec. 2 we recall expressions for the loop-generated Wilson coefficients from box and penguin diagrams. We provide the quantum numbers of the particles entering the loops and estimate the characteristic size of the couplings required to fit the flavor anomalies. In Sec. 3 we enlist the complete set of constraints we apply to the models. Section 4 is dedicated to the main results, with a description of the fitting procedure and discussion of the allowed parameter space. We present our conclusions in Sec. 5. Appendix A is dedicated to the detailed treatment of the recasting procedure for $B \rightarrow K + \text{inv.}$ limits.

2 Effective one-loop Wilson coefficients from split dark sector models

Our goal is to investigate to what extent the $b - s$ flavour anomalies can be explained by generic loop effects involving *light* new particles (in association with a heavy sector above the EWSB scale). Possible constructions for the Wilson coefficients of the effective Hamiltonian descending from loops of TeV-scale new particles have been investigated, e.g., in refs. [39–46]. They generally involve either box diagrams of scalar and fermionic states like in Fig. 1(a), or penguin diagrams like the ones represented in Fig. 1(b).

2.1 Box diagrams

If direct Yukawa couplings between the quarks b, s , the muons, and a NP sector composed of fermions ψ_i and scalars ϕ_j are allowed by the gauge quantum numbers, the most generic

Lagrangian is given by

$$\begin{aligned} \mathcal{L} \supset \bar{\psi}_i & \left(Y_{L,ij}^{(b)} P_L b + Y_{L,ij}^{(s)} P_L s + Y_{L,ij}^{(\mu)} P_L \mu \right) \phi_j \\ & + \bar{\psi}_k \left(Y_{R,kl}^{(b)} P_R b + Y_{R,kl}^{(s)} P_R s + Y_{R,kl}^{(\mu)} P_R \mu \right) \phi_l + \text{H.c.}, \end{aligned} \quad (2.1)$$

where a sum over repeated indices is implied. It was shown, e.g., in refs. [39, 40, 46, 47] that box diagrams like the one depicted in Fig. 1(a) can then contribute to the $B \rightarrow K^{(*)} \mu^+ \mu^-$ decay and one can construct out of Eq. (2.1) Wilson coefficients $C_9^{(\prime)\mu}, C_{10}^{(\prime)\mu}$ of the right order of magnitude to fit the anomalies. On the other hand, these box-like constructions do not generally involve light particles or very split spectra, as they would incur strong tension with several existing bounds.

Since at least one of the fermion or scalar fields in the box must necessarily carry the colour charge, the bounds from LHC searches for colour production with b -tagged jets will contribute to push this state above the 1 – 1.2 TeV scale [48–51]. At the same time there exist strong bounds from the measurement of B_s mixing [52] that either limit the available size of the Yukawa couplings or push one of the new states coupled to b, s to a very large scale. The strength of the B_s -mixing bound is very model-dependent and, if the particle content of the model at hand is large enough, cancellations between different diagrams can be engineered to evade the limit. Nevertheless, we can easily obtain an estimate of the B_s -mixing bound in minimal cases, when the particle content is just about right to fit the flavour anomalies via a box diagram similar to Fig. 1(a). Assuming that the colour charge is carried by particle 4 in the figure¹ we get, following, e.g., ref. [40], $|Y_{L,24}^{(b)} Y_{L,34}^{(s)*}| \lesssim 0.09$ at the 2σ level.

If particle 4 carries colour, the other states can in principle be lighter: $m_1 \approx m_2 \approx m_3 \lesssim m_4 \approx \mathcal{O}(\text{TeV})$. The Wilson coefficient C_9^μ is then approximately calculated as (see, e.g., refs. [40, 46])

$$C_9^\mu \approx - \frac{Y_L^{(s)*} Y_L^{(b)} |Y_{L,R}^{(\mu)}|^2}{(m_4/\text{TeV})^2} F(x, y, z), \quad (2.2)$$

where we have suppressed the subscript indices in the Yukawa couplings to lighten the notation, we define $x = (m_1/m_4)^2$, $y = (m_2/m_4)^2$, $z = (m_3/m_4)^2$, and F is a loop function,

$$F(x, y, z) = \frac{x^2 \ln x}{(x-1)(x-y)(x-z)} + \frac{y^2 \ln y}{(y-1)(y-x)(y-z)} + \frac{z^2 \ln z}{(z-1)(z-x)(z-y)}, \quad (2.3)$$

which equals approximately 1 when $m_1 \approx m_2 \approx m_3 \approx \mathcal{O}(100 \text{ GeV})$. As was shown in, e.g., refs. [39, 40, 46, 47], it follows from Eq. (2.2) that $C_9^\mu \lesssim -0.6$ requires Yukawa couplings $|Y_{L,R}^{(\mu)}| \gtrsim 3$ for $m_1 \approx m_2 \approx m_3 \approx \mathcal{O}(100\text{s GeV})$, a condition that does not guarantee the validity of perturbation theory up to scales much larger than EWSB.

¹The opposite choice would imply that particles 1, 2, and 3 carry colour, which in turn would lead to most states in the loop being either at the TeV scale or, in fact, SM quarks. While the latest possibility is interesting, it would trigger very strong tree-level flavour-violating bounds whose effect are likely to dominate the loop-induced signatures we consider here.

One might wonder at this point if an eventual light sector in the theory can provide a more natural fit to the flavour anomalies, perhaps requiring smaller Yukawa couplings to the muons. In fact, one infers from Eq. (2.3) that F can receive a logarithmic enhancement of a few units if x , y , and z are all at the same time significantly smaller than 1. But at least one among m_1 , m_2 , m_3 cannot be much smaller than m_4 . There are two reasons for this. First and foremost, multi-lepton searches at the LHC via Drell-Yan production constrain the particles carrying $SU(2)_L \times U(1)_Y$ quantum numbers to masses above the 400–600 GeV range [53–55]. On the other hand, if one were to roughly extrapolate a similar reasoning to m_1 , m_2 , m_3 smaller than the mass of the muon, so that the corresponding particles may possibly result invisible at the LHC, these would still necessarily contribute at one loop to the anomalous magnetic moment of the muon. The measured 2σ upper bound, $\delta(g-2)_\mu \lesssim 4 \times 10^{-9}$ [56–58] implies that the muon Yukawa coupling cannot be larger than

$$|Y_{ij,L(R)}^{(\mu)}| \lesssim 10^{-2} \left(\frac{m_{1,2,3}}{\text{GeV}} \right), \quad (2.4)$$

quite independently of the specifics of the model at hand.

A rough comparison of the typical size of Eq. (2.2) and Eq. (2.4) shows that the latter is too small to fit the flavour anomalies unless $m_{1,2,3}$ lie in the few hundreds of GeV or above. We conclude that there is arguably no common parameter space for $b \rightarrow s$ anomalies and $(g-2)_\mu$ with perturbative Yukawa couplings and a minimal, light NP sector, if the contributions to B decays stem from this class of box diagrams.

2.2 Penguin diagrams

It is more promising to look at another type of loop-induced coupling giving rise to the effective operators $\mathcal{O}_9^{(\prime)}$, $\mathcal{O}_{10}^{(\prime)}$: the penguin-diagram generated interaction. The penguin is constructed out of a loop with new fermion and scalar fields exchanging a vector boson with the leptons. If the vector boson is one of the SM gauge bosons, the contribution to $C_9^{(\prime)}$, $C_{10}^{(\prime)}$ is flavour-universal, and cannot be used to explain the LFUV anomalies. We will therefore be interested in models realising the penguin diagram topology presented in Fig. 1(b), in which a new light gauge boson V couples to the muons.

The particle that carries the colour charge in the loop might be a scalar multiplet Φ or a heavy VL fermion Ψ . In the former case we close the loop with a light (Dirac) fermion χ , whereas in the latter with a light scalar π . In order to avoid charging the b and s quarks under the dark gauge group $U(1)_D$ (with gauge coupling g_D), we assume that the dark charge is confined within the loop, i.e., $Q_{\chi(\pi)} = -Q_{\Phi(\Psi)}$. We thus avoid the strong bounds on V from multi-lepton searches at the LHC.

Without much loss of generality we will focus henceforth on the case where the heavy coloured particle is Φ . The case with Ψ does not present very significant differences, barring an order-one suppression of the amplitude that comes from swapping the role of the light and heavy mass in the loop functions. We thus introduce a scalar doublet $\Phi = (\phi_u, \phi_d)^T$ and a few light fermion singlets χ_i , whose multiplicity will be specified case by case. Explicitly, their $SU(3)_c \times SU(2)_L \times U(1)_Y \times U(1)_D$ quantum numbers read

$$\Phi = (\mathbf{3}, \mathbf{2}, 1/6, Q_\Phi) \quad \chi_i = (\mathbf{1}, \mathbf{1}, 0, -Q_\Phi).$$

Note that with the above charge assignment the mass matrix of the dark fermions is not a priori diagonal, unless the off-diagonal entries are forbidden by a flavour symmetry, or suppressed by some other mechanism. We will assume for simplicity that this is always the case, without entering in the specifics of such constructions.

We confine ourselves to the treatment of left-handed $b - s$ currents, in agreement with the findings of the global fits in the literature. Below the EWSB scale the Lagrangian of the hadronic NP sector reads

$$\mathcal{L} \supset y_d^{ij} \phi_d^* \bar{\chi}_i P_L d_j + y_u^{ij} \phi_u^* \bar{\chi}_i P_L u_j + \text{H.c.}, \quad (2.5)$$

where a sum over repeated indices is implied, and the Yukawa couplings are related by $y_u^{ij} = y_d^{ik} (V_{\text{CKM}}^\dagger)^{kj}$. We further confine ourselves to the basis where the only nonzero Yukawa couplings of the down-like type are those of the second and third generation: $y_d^{ik=1,2,3} = (0, y_s^i, y_b^i)^T$.

We finally introduce an effective interaction of the new gauge boson to the muons:

$$\mathcal{L} \supset (g_\mu^V \bar{\mu} \gamma_\nu \mu + g_\mu^A \bar{\mu} \gamma_\nu \gamma_5 \mu) V^\nu. \quad (2.6)$$

The relative size of the g_μ^V and g_μ^A couplings is governed by the UV model building and so is the eventual size, if nonzero at all, of the coupling of the new gauge boson to neutrinos. This point is of particular relevance when it comes to the constraints on the model from neutrino trident production [59] at CCFR [60] and CHARM-II [61], to which we come back in Secs. 3 and 4. We shall see that, while it is desirable to embed the effective model in a framework with forbidden or strongly suppressed couplings to the neutrinos,² we are able to find in our numerical analysis some viable parameter space lying below the bound from CCFR and CHARM-II.

We calculate the penguin diagram contributions to the $B_s \rightarrow K^{(*)} \mu^+ \mu^-$ decay. Following standard techniques one obtains an amplitude that closely resembles the SM photon penguin case, with a slight modification due to the Breit-Wigner distribution of the massive gauge boson V . Estimating the loop diagram is equivalent to integrating out the heavy colour-charged field, which generates the dimensionful Wilson coefficient \tilde{g} of the operator

$$\mathcal{O}_6 = (\bar{s} \gamma_\rho P_L b) \partial_\sigma V^{\rho\sigma}, \quad (2.7)$$

where $V^{\rho\sigma} = \partial^\rho V^\sigma - \partial^\sigma V^\rho$ [34, 35]. We find

$$\tilde{g} = -\frac{g_D Q_\Phi}{16\pi^2 m_\Phi^2} \sum_i y_s^{i*} y_b^i \mathcal{F}(x_i), \quad (2.8)$$

²For example, one can construct a Type-I 2-Higgs doublet model where the additional Higgs doublet and extra VL heavy leptons all carry $U(1)_D$ charge: $\Theta : (\mathbf{1}, \mathbf{2}, 1/2, Q_\Theta)$, $E : (\mathbf{1}, \mathbf{1}, 1, Q_\Theta)$. Yukawa couplings with the SM left-handed muon doublet L_μ , of the type $\lambda \Theta^\dagger L_\mu E$, generate a left-chiral coupling g_μ^L of V to the muons once $U(1)_D$ is broken. The coupling to neutrinos is absent. Typically one gets $g_\mu^L \approx -g_D Q_\Theta \lambda v_\Theta^2 / 2m_E^2$. More than one family of VL singlet fermions, and an additional complex scalar singlet charged under $U(1)_D$ can be introduced to generate the right-chiral couplings and to push the mass of the scalars with electric charge above the current bound from LEP and LHC searches [62].

where we have defined $x_i = m_{\chi_i}^2/m_\Phi^2$ and the loop function reads

$$\mathcal{F}(x) = -\frac{1}{2} - \frac{1}{3} \ln x. \quad (2.9)$$

The contribution of \mathcal{O}_6 to the $B \rightarrow K$ processes mediated by the exchange of a vector boson can be related to “effective” Wilson coefficients $C_{9,10}^\ell$ as

$$C_{9(10)}^\mu(q^2) = -\frac{4\pi\mathcal{N}}{\alpha_{\text{EM}}} \tilde{g} g_\mu^{V(A)} \frac{q^2}{q^2 - m_V^2 + im_V\Gamma_V}, \quad (2.10)$$

where m_V is the mass of the gauge boson, we define

$$\mathcal{N}^{-1} = \frac{4G_F}{\sqrt{2}} V_{tb} V_{ts}^*, \quad (2.11)$$

and Γ_V is the total width of the gauge boson, which reads, when all light decay channels are kinematically open,

$$\Gamma_V = m_V (\gamma_V^D + \gamma_V^\mu), \quad (2.12)$$

with the dark fermion and SM muon contributions respectively given by

$$\gamma_V^D = \frac{1}{12\pi} \left[\sum_i \sqrt{1 - \frac{4m_{\chi_i}^2}{m_V^2}} \left(\frac{2m_{\chi_i}^2}{m_V^2} + 1 \right) g_D^2 Q_\chi^2 \right], \quad (2.13)$$

$$\gamma_V^\mu = \frac{1}{12\pi} \left[\sqrt{1 - \frac{4M_\mu^2}{m_V^2}} \left(\frac{2M_\mu^2}{m_V^2} + 1 \right) (g_\mu^V)^2 + \left(1 - \frac{4M_\mu^2}{m_V^2} \right)^{3/2} (g_\mu^A)^2 \right]. \quad (2.14)$$

Note that the Wilson coefficient \tilde{g} , similarly to $C_{9(10)}(q^2)$, does not run at the leading order in QCD, since its colour part is simply a vector current [63].

To facilitate a comparison with the existing literature, we further define the dimensionless coupling of V to the $b-s$ current, g_{Vbs} , as

$$g_{Vbs} \equiv -\tilde{g} q^2. \quad (2.15)$$

The typical size of g_{Vbs} is shown in Fig. 2 for representative choices of the input parameters. For illustration purposes, we have set q^2 to the indicative scale of 3.5 GeV^2 . Note, however, that in the phenomenological analysis of Sec. 4 we integrate Eq. (2.10) over all the relevant invariant-mass bins.

Equation (2.10) shows that the penguin-generated Wilson coefficients depend on q^2 and the size of the width of the new gauge boson. They enter nontrivially in the calculation of the flavour observables and relative constraints when the V mass lies in the vicinity of the experimental bins. The corresponding expressions should thus be compared directly to the experimental data, as we do in the numerical scan presented in Sec. 4. We can nonetheless provide a rough estimate of the typical size required for the dimensionful coupling \tilde{g} in the limiting cases when m_V becomes much larger or much smaller than the experimental

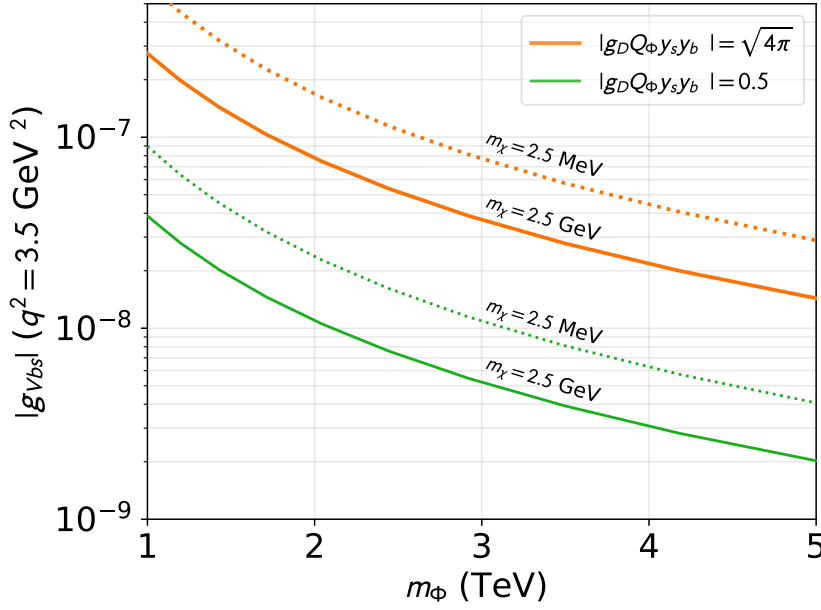


Figure 2: The typical size of g_{Vbs} as a function of the heavy mass m_{Φ} for different choices of the effective coupling $|g_{DQ\Phi y_s^{i*} y_b^i}|$ given here for one light dark fermion, χ_1 . Solid (dashed) lines correspond to $m_{\chi_1} = 2.5$ GeV(MeV). Indicative momentum transfer is set at $q^2 = 3.5$ GeV².

energy (for the LFUV observables we indicatively consider this to be $q^2 \approx 0.04 - 8$ GeV²). If $m_V \gg 10$ GeV one obtains $C_9^\mu \lesssim -0.6$ roughly for

$$|\tilde{g} g_\mu^V| \gtrsim 1 \times 10^{-10} \frac{m_V^2}{\text{GeV}^4}, \quad (2.16)$$

where we have set q^2 at the mean momentum transfer for the $1 - 6$ GeV² bin of the $R_{K^{(*)}}$ observables.

The two couplings \tilde{g} and g_μ^V are independently constrained by two powerful probes. On the one hand, the measured 2σ bound on R_{BB} from B_s mixing [52] has a direct impact on \tilde{g} when the vector V is exchanged in the s -channel:³

$$|\tilde{g}| \lesssim 7 \times 10^{-8} \frac{m_V}{\text{GeV}^3}, \quad (2.17)$$

where the characteristic experimental scale coincides with the B_s mass, $q^2 = M_{B_s}^2$.

On the other hand, the already mentioned 2σ upper bound on the anomalous magnetic moment of the muon constrains g_μ^V to

$$|g_\mu^V| \lesssim 7 \times 10^{-3} \frac{m_V}{\text{GeV}}. \quad (2.18)$$

³Note, however, that g_{Vbs} depends directly on the product $y_s^{i*} y_b^i$, which produces box diagrams that are also contributing to B_s mixing, and might result on a stronger bound than the one derived by s -channel exchange of V . We will come back to this point in Sec. 3.

The current bounds thus result in a very narrow window of availability for explaining the flavour anomalies with penguin diagrams and $m_V \gg 10 \text{ GeV}$.

At the opposite side of the spectrum, $m_V < 200 \text{ MeV}$, the new gauge boson is much lighter than the experimental energy scale. Equation (2.10) shows that the Wilson coefficients become independent of m_V and of q^2 . $C_9^\mu \lesssim -0.6$ requires approximately

$$|\tilde{g} g_\mu^V| \gtrsim 5 \times 10^{-10} \text{ GeV}^{-2}. \quad (2.19)$$

The most severe constraint in this mass range comes again from the 2σ upper bound on the anomalous magnetic moment of the muon, which requires

$$|g_\mu^V| \lesssim 0.6 - 1 \times 10^{-3}, \quad (2.20)$$

where the upper value refers essentially only to the region $m_V \gtrsim 100 \text{ MeV}$, and the lower value to all other masses below that. In light of Eqs. (2.19) and (2.20) one needs $|\tilde{g}| \gtrsim 10^{-6} \text{ GeV}^{-2}$ to fit the flavour anomalies. As one can see in Fig. 2, effective couplings of this size are not easy to obtain in the penguin setup.

It is well known (cf., e.g., ref. [33]) that one can increase the size of g_μ^V while respecting the 2σ upper bound on $(g-2)_\mu$ by introducing the axial-vector coupling g_μ^A and thus creating a negative contribution to $(g-2)_\mu$ that has to be fine-tuned. This, however, also induces an extremely strong contribution to the $B_s \rightarrow \mu\mu$ decay rate, and will prove ultimately impracticable, as will appear clear in the next sections.

Altogether, this discussion leads us to conclude that the most natural solutions are likely to be situated inside the window $m_V \approx 0.2 - 10 \text{ GeV}$. The remainder of this paper is thus dedicated mostly to this mass range. Note that when m_V approaches M_B , additional resonant enhancement can be obtained to open up the parameter space, albeit at the cost of additional limits from $B \rightarrow K$ processes, which we will describe in detail in the next section.

3 Constraints on the model

3.1 Flavour constraints

B_s -mixing Strong limits on the Yukawa couplings of Eq. (2.5) arise from box-diagram contributions to B_s -mixing. We recall that for exclusively left-handed couplings the only relevant operator is \mathcal{O}_1 [40, 46]. The corresponding dimensionful Wilson coefficient is defined as

$$C_1 = \frac{1}{128\pi^2 m_\Phi^2} \sum_{ij} y_s^{i*} y_b^i y_s^{j*} y_b^j F(x_i, x_j), \quad (3.1)$$

where the sum runs over all possible dark fermions $\chi_{i,j}$, out of which we can construct a box diagram with Φ . We define $x_{i(j)} = m_{\chi_{i(j)}}^2 / m_\Phi^2$ and the loop function reads

$$F(x, y) = \frac{1}{(1-x)(1-y)} + \frac{x^2 \log x}{(1-x)^2(x-y)} + \frac{y^2 \log y}{(1-y)^2(y-x)}. \quad (3.2)$$

In the small x, y limit, the loop function can be approximated as $F(x, y) \simeq 1$, so that $C_1 \propto 1/m_\Phi^2$ and the limit essentially saturates. This has the unexpected consequence that, in the presence of several dark fermion states, one can readily get a large suppression of the B_s -mixing contribution in the limit where $\sum_{ij} y_s^{i*} y_b^i y_s^{j*} y_b^j \ll 1$, which can be easily obtained with, e.g., two light states χ_1, χ_2 and $y_s^{1*} y_b^1 \approx -y_s^{2*} y_b^2$.

Note that while C_1 receives a strong suppression from the addition of approximately equal and opposite-sign couplings, there is no equivalent suppression for C_9^μ , as in the limit of small x_1, x_2 the effective coupling \tilde{g} in Eq. (2.15) becomes proportional to $\ln(x_1/x_2)$.

Limits from B_s decay When the axial-vector coupling to the muon, g_μ^A , is present, the vector mediator can induce a contribution to the decay $B_s \rightarrow \mu^+ \mu^-$ via the effective operator \mathcal{O}_6 , cf. Eq. (2.7). (Equivalently, via the effective $b - s - V$ coupling.) The decay amplitude is expressed in terms of “effective” coefficients C_{10} and C_P , whose contributions to $B_s \rightarrow \mu^+ \mu^-$ are well known [64–67].

By adopting the same convention for the scalar operator as in ref. [46] we obtain a result similar to [33]:

$$C_{10}(M_{B_s}^2) = \frac{4\pi\mathcal{N}}{\alpha_{EM}} \frac{M_{B_s}^2 \tilde{g} g_\mu^A}{M_{B_s}^2 - m_V^2 + im_V \Gamma_V}, \quad (3.3)$$

$$C_P(M_{B_s}^2) = -\frac{2M_\mu(M_b + M_s)}{m_V^2} C_{10}(M_{B_s}^2). \quad (3.4)$$

The typical bounds on C_P are significantly more stringent than those on C_{10} . They are likely to have a strong impact on our results so that we include them directly in the full numerical scan present in the next section.

Limits from $B \rightarrow K^{(*)}$ transitions Depending on the details of the UV completion there can exist additional $B \rightarrow K^{(*)}$ decays providing strong constraints on our model. The two main limits are (1) invisible $B \rightarrow K$ transition measured by BaBar [68, 69] and Belle [70, 71], $\mathcal{BR}(B \rightarrow K \nu \nu) \lesssim 1.5 \times 10^{-5}$; and (2) resonant search $B \rightarrow K^* V$, $V \rightarrow \mu \mu$ measured at LHCb [72], which constrains the branching ratio $\mathcal{BR}(B \rightarrow K^* V, V \rightarrow \mu \mu) \lesssim 2 \times 10^{-9}$.

Given the presence of the heavy scalar doublet Φ and one dark fermion χ_1 , one can construct the tree-level decay process $B \rightarrow K \chi_1 \chi_1$ based on the b quark 3-body decay $b \rightarrow \chi_1 \Phi^* \rightarrow s \chi_1 \chi_1$. In the limit where $m_{\chi_1}, M_K \ll M_B$, we have the simple expression:

$$\Gamma_{K \chi_1 \chi_1}^{\text{tree}} \approx \frac{f_+^2 |y_s^1|^2 |y_b^1|^2}{1536 \pi^3} \frac{M_B^5}{m_\Phi^4}, \quad (3.5)$$

where $f_+^2 \approx 0.3$ is the average value of the form factor over the range of integration of the differential decay rate. This typically leads to the constraint $|y_s^{1*} y_b^1| \lesssim 10^{-2} (m_\Phi/\text{TeV})^2$ on the Yukawa couplings of any new fermion with mass $2m_{\chi_1} < M_B - M_K$. As Eq. (2.15) shows, the upper bound on the Yukawa couplings strongly limits the available range of g_{Vbs} , even when the gauge coupling g_D is large. This means that to fit the flavour observables one has to resort to a large g_μ^V value, which, as we shall see in Sec. 4, is severely constrained by

Z -lineshape bounds (in addition to requiring a fine tuning of the axial-vector contribution to avoid exceeding $\delta(g-2)_\mu$). To avoid these problems the minimal particle content will have to include at least one dark fermion with mass $m_{\chi_1} > (M_B - M_K)/2$.

On the other hand, there is a case to be made for the presence of additional light states with mass below the $(M_B - M_K)/2$ threshold and Yukawa couplings to Φ and the b and s quarks that are small enough to avoid the tree-level $B \rightarrow K + \text{inv.}$ bound.

- *Dark matter* For a fermion χ_1 of mass above the $(M_B - M_K)/2$ threshold the direct s -wave annihilation channel, $\chi_1 \chi_1 \rightarrow V \rightarrow \mu^+ \mu^-$, is strongly constrained by CMB bounds [73]. Introducing one additional lighter state χ_0 with the same quantum numbers provides instead a viable candidate for *forbidden* dark matter (we come back to this point in more detail at the end of Sec. 4)
- The presence of additional light states directly affects the total width of the gauge boson V , potentially opening up additional parameter space for a solution to the flavour anomalies.

In cases where at least one light state χ_0 appears besides χ_1 , two qualitatively different regimes of applicability should be considered for the invisible $B \rightarrow K$ transition. For fermions not very light and $m_V < 2M_\mu < M_B - M_K < 2m_{\chi_{i=0,1}}$, *on-shell* decay $B \rightarrow KV$ occurs, in which V escapes undetected. It is typically suppressed in the low m_V limit due to the momentum dependence of the effective coupling g_{Vbs} defined in Eq. (2.15). We get

$$\Gamma_{KV} = f_+^2(m_V) \tilde{g}^2 \frac{m_V^2 M_B^3}{64\pi} \lambda(1, x_K, x_V)^{3/2}, \quad (3.6)$$

where we have assumed $m_V, M_K \ll M_B$, $f_+(0) \simeq 0.3$ is a form factor (the full expression, used in the numerical analysis of Sec. 4, can be found in ref. [74]), and $\lambda(x, y, z) = (x - y - z)^2 - 4xy$ is the standard Källén (triangle) function with $x_K = M_K^2/M_B^2$, $x_V = m_V^2/M_B^2$.

On-shell decays $B \rightarrow K \chi_0 \chi_0$, occurring when $2m_{\chi_0} < m_V < M_B - M_K$, require Eq. (3.6) to be multiplied by the branching ratio $\mathcal{BR}(V \rightarrow \chi_0 \chi_0)$. An additional channel is opened via the exchange of a virtual V and it can dominate the invisible decay width when m_V is small and the dark coupling g_D is large. The full width reads

$$\Gamma_{K\chi_0\chi_0} = \int_{4M_\mu^2}^{(M_B - M_K)^2} ds \frac{\sqrt{s}}{\pi} \frac{\Gamma_{V \rightarrow \chi_0 \chi_0}(s) \Gamma_{KV}(s)}{m_V^2 \Gamma_V^2 + (m_V^2 - s)^2}, \quad (3.7)$$

where $\Gamma_{KV}(s)$ and $\Gamma_{V \rightarrow \chi_0 \chi_0}$ are obtained by replacing m_V by \sqrt{s} in Eq. (3.6) and in the corresponding V decay width to fermions, and Γ_V is the total width of V , cf. Eq. (2.12). Note that with more than one dark fermion in the spectrum one ought to sum over all individual off-shell contributions.

Altogether, the combination of both real and virtual contribution to the $B \rightarrow K \chi_0 \chi_0$ decay implies a complex kinematic shape in terms of missing energy, which may differ significantly from the SM-like $B \rightarrow K \nu \nu$ decay. This has the direct consequence that the experimental results of Belle and BaBar, which are optimised for the neutrino process, should not be directly applied to our scenario. We therefore perform a conservative recasting of these analyses, described in detail in Appendix A.

Finally, in the mass regime $m_V > 2M_\mu$, the light vector state can directly decay into a muon pair and this opens up the resonant channel $B \rightarrow K^*V$, $V \rightarrow \mu\mu$. This is especially important if one restricts the analysis to the case with only one dark fermion χ_1 with $2m_{\chi_1} > M_B - M_K$. The typical decay width into K^* is given by

$$\Gamma_{K^*V} = \frac{\tilde{g}^2 m_V^2 M_B^5}{64\pi M_{K^*}^2 (1 - x_{K^*})^2} \sqrt{\lambda(1, x_{K^*}, x_V)} \mathcal{F}_1(x_{K^*}, x_V), \quad (3.8)$$

where an explicit expression for $\mathcal{F}_1(x_{K^*}, x_V)$ can be found in Appendix B of ref. [35]. Note that in the limit where $m_V \ll M_B$, $\mathcal{F}_1(x, y)$ simplifies to $\mathcal{F}_1(x, y) \simeq 0.1\sqrt{x}(y + 1.2x)$, so that Γ_{K^*V} is typically suppressed compared to Γ_{KV} . Furthermore, the branching ratio to muons is inversely proportional to the total width Γ_V and can thus be strongly suppressed if the coupling of V to extra dark fermions χ_i is large.

Note that the limits from LHCb [72] on this process focused on a narrow, or even long-lived, new resonance, with limits based on invariant mass bins of a few MeV. This hypothesis is especially problematic when the mediator is around the GeV range, since a large dark gauge coupling implies a very large width for V . We then simply model the resonance via a Breit-Wigner distribution and compare bin-by-bin with the limit of ref. [72], retaining the strongest bin as the main limit.⁴

The overall impact of the limits from $B \rightarrow K^{(*)}$ transitions on the size of the effective coupling g_{Vbs} is summarised in Fig. 3 as a function of the vector mass m_V , for three representative choices of the pair (m_{χ_0}, g_D) . For $m_{\chi_0} = 5 \text{ GeV}$, the decay $B \rightarrow K\chi_0\chi_0$ is kinematically forbidden, so that invisible B decays can only proceed via the on-shell process $B \rightarrow KV$. This results in a weak bound in the small m_V regime (blue line). Note that when $m_V > 2M_\mu$, the constraints from resonant searches using $B \rightarrow K^*\mu\mu$ strongly exclude this setup since $V \rightarrow \mu\mu$ is in this case the only accessible decay channel.

In the presence of dark fermions with a small mass, $2m_{\chi_0} < M_B - M_K$, the decay channel $V \rightarrow \chi_0\chi_0$ opens up and the relative strength of different bounds depends on the size of g_D . In the case of large g_D (orange line), if $2m_{\chi_0} < m_V < M_B - M_K$ both the on-shell and off-shell invisible decays contribute to the width. For light vector mediator the off-shell decay takes over due to the q^2 dependence of the coupling and the bound on g_{Vbs} saturates. If, on the other hand, g_D is smaller (green line) and $m_V > 2M_\mu$, the constraints from resonant searches using $B \rightarrow K^*\mu\mu$ typically overcome the invisible decay limits, suppressing g_{Vbs} by an order-one factor.

Finally, note that for large m_V the limit arises from invisible searches from the off-shell decay $B \rightarrow K\chi_0\chi_0$ when it is kinematically allowed.

⁴While it is clear that a complete recasting of the LHCb analysis [72] for a large-width NP signal would impact the $\sim \text{GeV}$ mass range of V , we do not expect significant modifications to the overall picture discussed in Sec. 4 since: (1) limits on $\mathcal{BR}(B \rightarrow K + \text{inv.})$ *already* forbid scan points compatible with the flavour anomalies in this region when the invisible width is large; (2) this region has a strong background from the charm-quark resonances [33]; and (3) we already include the main flavour observable in the numerical scan via the differential branching ratio of $B \rightarrow K\mu\mu$.

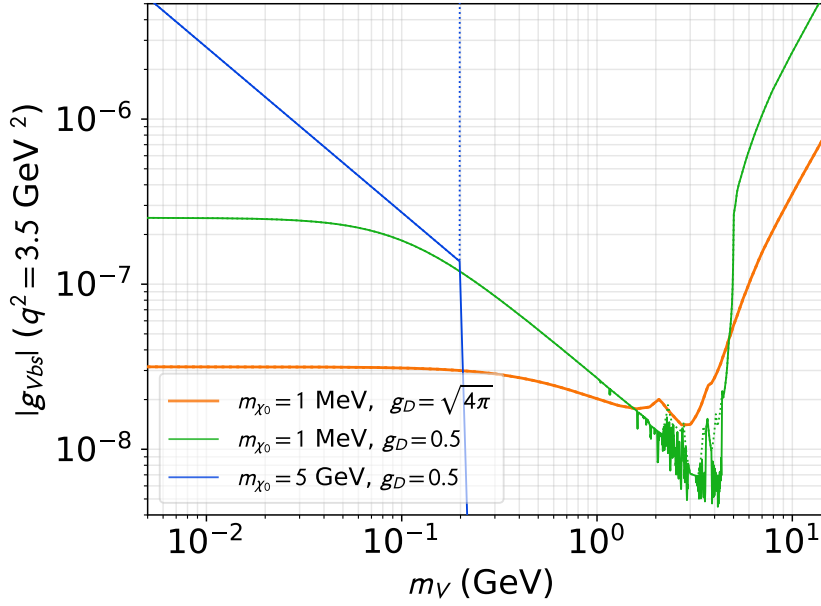


Figure 3: Upper bound on $|g_{Vbs}(3.5 \text{ GeV}^2)|$ as a function of m_V for various choices of the input parameters. We set $Q_\Phi = 1$. The specific impact of the different constraints is described in the main text.

3.2 Precision physics constraints

Muon anomalous magnetic moment The couplings of V to muons can be constrained by the measurement of the anomalous magnetic moment of the muon. A contribution to $(g - 2)_\mu$ is in this case given by [75, 76]

$$\delta(g - 2)_\mu = \frac{1}{8\pi^2} \frac{M_\mu^2}{m_V^2} \mathcal{F}\left(\frac{M_\mu}{m_V}\right), \quad (3.9)$$

where

$$\mathcal{F}(x) = \int_0^1 dz \frac{(g_\mu^V)^2 2z^2(1-z) + (g_\mu^A)^2 [2z(1-z)(z-4) - 4x^2z^3]}{x^2z + (1-z)(1-x^2z)}. \quad (3.10)$$

As was mentioned in Sec. 2, given the limited range achievable in penguin constructions for g_{Vbs} , when only vector-like couplings to the muons are present it becomes difficult to find a g_μ^V value large enough to allow for a reasonable agreement with the flavour anomalies and at the same time not too large a deviation from the measured value of $(g - 2)_\mu$. A certain level of cancellation with the contribution from the axial-vector coupling must take place in most situations [33]. For a GeV-scale vector mediator, this occurs for $g_\mu^A \approx -0.44 g_\mu^V$. Note, however, that including the axial-vector contribution triggers the strong bounds from $B_s \rightarrow \mu\mu$ discussed above.

Z physics and intensity frontier limits The coupling of the Z boson to the muon is modified at the one-loop level [77, 78] within UV constructions of the type as in Footnote 2. However, due to the smallness of the Z -boson coupling to charged leptons in the SM, the limit is typically subdominant with respect to the $(g - 2)_\mu$ bound.

A powerful method for discerning light resonances through precision measurements of Drell-Yan dimuon production was proposed in ref. [79]. For $m_V = 1 - 5$ GeV an upper bound can be derived

$$\sqrt{(g_\mu^V)^2 + (g_\mu^A)^2} \lesssim 5.6 \times 10^{-2} \left(1 + 0.13 \frac{m_V}{\text{GeV}}\right). \quad (3.11)$$

Finally, the Belle-II Collaboration recently provided a bound on the final state radiation process $e^+e^- \rightarrow \mu^+\mu^-V$, $V \rightarrow$ invisible, based on 0.28 fb^{-1} of data from the 2018 run [80], which applies directly to our model. While the current limit can hardly compete with the Drell-Yan bound, the 2019 run has stored $\sim 10 \text{ fb}^{-1}$ and moreover a few ab^{-1} should be obtained in 2020, so that future data will become rapidly relevant.

Notice that more generically, for a V mass above ~ 10 GeV, the phenomenology of the light fermions in intensity frontier experiments can be obtained by integrating it out and considering the fermion portal four-fermion operators [81]. Similarly, the limit from the tree-level $b \rightarrow \chi \Phi^* \rightarrow s \chi \chi$ decay can also be obtained by integrating out the heavy scalar Φ and using the existing bounds on the fermion portal operator $\bar{b} \gamma^\mu s \bar{\chi} \gamma_\mu \chi$. While we cover directly the relevant limits in this section, the latter approach could be particularly fruitful to study and constrain the possible couplings between new light fermions and the other SM generations.

Neutrino trident production If the gauge boson features a coupling g_ν to muon neutrinos (cf. Sec. 2.2), one expects a strong enhancement in the neutrino trident production from scattering on atomic nuclei, $N: N\nu \rightarrow \nu N \mu^+ \mu^-$ [59].

The cross section for this process has been measured by the CCFR [60] and CHARM-II [61] collaborations to be in agreement with the SM prediction. In the range $m_V > 1$ GeV it results in the generic bound

$$g_\nu \lesssim 0.002 \left(\frac{m_V}{\text{GeV}}\right), \quad (3.12)$$

which roughly saturates for smaller mass to about $g_\nu \lesssim 0.001$.

When the bound appears in the plots of Sec. 4 it is obtained under the assumption $g_\nu \equiv g_\mu^V$ (we repeat that whether or not the bound is relevant depends on the UV completion).

Kinetic mixing In presence of states charged both under the $U(1)_Y$ and $U(1)_D$ symmetry groups, kinetic mixing ϵ between the photon and the vector V will be generated at the loop level. The corresponding 1-loop contributions from fermions and scalars are given by

$$\epsilon \approx \frac{g_D g_Y \cos \theta_W}{12\pi^2} \left(\sum_{f \in \text{ferm.}} N_{3f} Y_f Q_f + \frac{1}{8} \sum_{s \in \text{scal.}} N_{3s} Y_s Q_s \right), \quad (3.13)$$

where $Y_{f,s}$ is the fields' hypercharge, $Q_{f,s}$ is the dark charge, and the coefficients $N_{3f,s}$ indicate the dimension of the $SU(3)_c$ representation.

The fields that contribute to the kinetic mixing are Φ , μ_L , and μ_R which, when $g_\mu^{V,A} \ll g_D$, results in

$$\epsilon \approx 8 \cdot 10^{-4} \times \left(\frac{g_D}{3} \right). \quad (3.14)$$

Such a kinetic mixing is at the limit of exclusion given the current intensity frontier searches (see, e.g., ref. [82] for a recent review), especially when invisible decay channels are not available for the vector mediator. However, the precise value of the kinetic mixing is strongly dependent on the UV physics, and additional VL fields can modify the prediction of Eq. (3.13) although not by many orders of magnitude.

LHC constraints on $t \rightarrow c\mu\mu$ We work in this paper under the assumption that the only nonzero Yukawa couplings of the down-like type are y_s^i , y_b^i . However, as Eq. (2.5) shows, the corresponding Yukawa couplings of the up-like type, y_c^i , y_t^i , do not receive CKM suppression. They can thus generate non-negligible contributions to processes involving $t \rightarrow c\mu\mu$ transitions.

Effective operator analyses of LHC bounds from rare top decays [83, 84], derived originally for the very-high mass regime, $m_V \sim \mathcal{O}(\text{TeV})$, impose a fairly weak bound on the coupling product when $m_V \ll M_t$:

$$|\tilde{g} g_\mu^V| \lesssim 10^{-6} \text{ GeV}^{-2}. \quad (3.15)$$

A rough comparison with Eq. (2.16) shows that this is not likely to be constraining for our scenarios. However, given that Eq. (2.10) presents a nontrivial q^2 dependence, for the light mass range investigated in this paper one should rather perform a detailed recast of the experimental searches. This task exceeds the purpose of the present paper in view of the fact that, as we will show in Sec. 4, the flavour and intensity frontier experiments discussed above provide already a set of powerful and often inescapable constraints on the dark sector.

4 Fitting procedure and results

Fitting procedure We perform a multidimensional fit of the following free parameters: m_V , g_μ^V , $r_{AV} \equiv g_\mu^A/g_\mu^V$, γ_V^D , $r = g_D Q_\Phi y_s^{1*} y_b^1$ (with only one light dark fermion χ_1 contributing with Yukawa couplings y_s^1 and y_b^1). r is employed here as a proxy for the effective coupling \tilde{g} once the mass parameters are fixed. We choose $m_{\chi_1} = 2.5 \text{ GeV}$ and $m_\Phi = 1 \text{ TeV}$; under these assumptions r relates to \tilde{g} as $|\tilde{g}| = |2.2 \times 10^{-8} \text{ GeV}^{-2} r|$. Since the fitted flavour observables depend on \tilde{g} rather than the couplings composing it, our results can be extended straightforwardly to the case with more light fermions.

The prior ranges of the fitted parameters are presented in Table 1. Separate fits are performed depending on whether m_V lies above or below the relevant bins for the B anomalies. In the text we refer to these sets as the *high-mass* fit and the *low-mass* fit. This is required by the fact that in order to obtain a negative C_9^μ the product $r \cdot g_\mu^V$ should assume a different sign in each of these two regions (we will come back to this point

Parameter	Prior range
$ r $	$[0.075, 25]$
g_μ^V	$[0.001, 0.2]$
γ_V^D	$[0.001, 0.4]$
r_{AV}	$[-1, 0]$
$m_V(\text{GeV})$	$[0.6, 2]$ and $[2, 15]$

Table 1: Prior ranges for the free parameters of the model. For the first three parameters the prior distribution is given in logarithmic scale, while for the others it is given in linear scale.

later on, when discussing our numerical results). We observe that $m_V = 2 \text{ GeV}$ gives an approximate threshold separating the two regimes.

We fit the free parameters of the model to the available experimental data reporting anomalies in B -meson decays, namely the LFUV ratios R_K , R_{K^*} , the angular observables in the $B \rightarrow K^* \mu^+ \mu^-$ decay and the branching ratio of $B_s \rightarrow \mu\mu$.⁵ In the high-mass regime we include in the likelihood function the experimental 2σ upper bound on the anomalous magnetic moment of the muon, $\delta(g-2)_\mu \lesssim 4 \times 10^{-9}$. We do not incorporate this bound in the likelihood function of the low-mass fit to avoid driving the scan too forcefully towards parameter space regions that are in tension with the remaining constraints.

To carry out the fit, we employ the `HEPfit` package [85], performing a Markov Chain Monte Carlo (MCMC) analysis by means of the Bayesian Analysis Toolkit (BAT) [86]. A set of $\mathcal{O}(500K)$ points is generated for the two scenarios described in Table 1, and for each case the subset of points reproducing the B anomalies, $\mathcal{BR}(B_s \rightarrow \mu\mu)$, and the upper $(g-2)_\mu$ bound (in the high-mass case only) at the 2σ level, is stored. These initial subsets of points are then subjected to additional constraints coming from B_s mixing, Drell-Yan production and, when applicable, $B \rightarrow K + \text{inv.}$ searches.

Results for high-mass We start with addressing solutions in the high-mass range, $m_V = 2 - 15 \text{ GeV}$.

Two dark fermions in the theory: $m_{\chi_0} \leq m_{\chi_1}$ We describe here a case in which the gauge boson V features a non-negligible invisible width, which could stem from the presence in the spectrum of an additional light fermion χ_0 besides χ_1 (see discussion in Sec. 3.1). The results of the scan in the (m_V, g_μ^V) plane are presented in Fig. 4. The yellow points are obtained in the scanning procedure described above and correspond to the models in which the B anomalies, $\mathcal{BR}(B_s \rightarrow \mu\mu)$, and $\delta(g-2)_\mu$ are fitted at the 2σ level. The green

⁵Due to the explicit q^2 dependence of $C_{9,10}^\mu$ it is not possible to match the Wilson coefficients to the model-independent bounds obtained by the global fits in the literature. Instead, $C_{9,10}^\mu$ have to be fitted directly to the experimental data. On the other hand, if m_V is in the MeV range, it is possible to directly match the Wilson coefficients to the model-independent bounds obtained by the global fits.

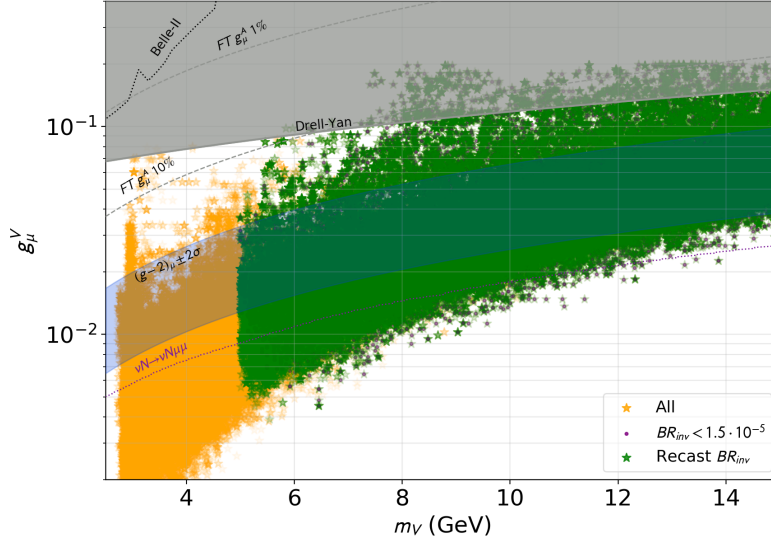


Figure 4: In yellow model points in which the $b \rightarrow s$ anomalies, $\mathcal{BR}(B_s \rightarrow \mu\mu)$, and $(g-2)_\mu$ are fitted at the 2σ level. Superimposed points are allowed after the limits from $B \rightarrow K + \text{inv.}$ are applied, as reported by CLEO [87] (purple) or using our recast procedure (green), cf. Appendix A. Grey shaded region is excluded by precision measurements of Drell-Yan at the LHC [79]. Purple dotted line indicates the exclusion bound from the neutrino trident production [59]. Dotted black line indicates the upper bound from Belle II [80]. In light blue we mark the region in which the $(g-2)_\mu$ constraint is satisfied at 2σ with $g_\mu^A = 0$.

points are those that remain allowed after the limits from $B \rightarrow K + \text{inv.}$ transitions are applied, following the recasting procedure outlined in Appendix A.

The on-shell process $B \rightarrow KV$, $V \rightarrow \chi_0\chi_0$ typically proceeds unsuppressed for a GeV-scale mediator, so that all the yellow points below the $M_B - M_K$ threshold are excluded. On the other hand, the limits on \tilde{g} are dramatically weakened above the $M_B - M_K$ threshold (see Fig. 3), so that in this regime one can easily fit simultaneously $(g-2)_\mu$ and the flavor anomalies. Incidentally, we find that solutions to the flavour anomalies with $m_V \approx 2.5$ GeV, corresponding to the case described in ref. [33], are excluded. The reason is that, unlike ref. [33], in our framework g_{Vbs} is q^2 -dependent and induces an $(m_V/\text{GeV})^2$ enhancement to the size of Eq. (3.6).

An additional bound on the parameter space of the model is derived from the Z line-shape from Drell-Yan at the LHC, which strongly affects the maximal allowed value of g_μ^V [79]. The corresponding exclusion region is depicted in Fig. 4 in dark grey. The shading is obtained under the assumption $g_\mu^A = -0.44 g_\mu^V$, a relation that induces destructive interference in the calculation of $(g-2)_\mu$ (cf. Eqs. (3.9) and (3.10)). It is well known [33] that the above relation between the vector and axial-vector coupling requires some level of fine tuning. The grey dashed lines in Fig. 4 trace the value of g_μ^V that corresponds to the

indicated level of fine tuning in $g_\mu^A \approx -0.44 g_\mu^V$ required to avoid exceeding the 2σ upper bound from the measurement of $\delta(g-2)_\mu$. Note, however, that the tuning of the vector and axial-vector muon couplings is a priori not needed in the high-mass regime, as confirmed by the large number of green points within the blue shaded band, corresponding to the region satisfying the $(g-2)_\mu$ constraint at 2σ with $g_\mu^A = 0$. This is an attractive feature of our model, in which we can obtain relative low values of g_μ^V and subsequently avoid the Drell-Yan limit.

In Fig. 4 the limits from the neutrino trident production derived in ref. [77] for $g_\mu^A = 0$ are shown as a dashed purple line. The constraint applies only if the mediator couples directly to neutrinos, cf. discussion in Sec. 2.2. It should be stressed that, even when the neutrino trident bound applies, solutions that escape the experimental limit exist, with $m_V = 5 - 14 \text{ GeV}$ and r at the upper end of the scanned range.

Finally, it is instructive to compare the results obtained within our UV-complete setup to those derived in simplified Z' models with an effective coupling to the $b-s$ current, g_{bs} . For example, a solution to the $b-s$ anomalies (without the $(g-2)_\mu$ constraint) was found in ref. [18], with $m_{Z'} = 10 \text{ GeV}$, $g_\mu^V = -g_\mu^A \approx 10^{-2}$, and $g_{bs} \approx 5 \times 10^{-6}$. Figure 4 shows that we obtain solutions characterised by similar mass and muon coupling in our setup, corresponding, again, to r values at the upper end of the scanned range.

One dark fermion χ_1 in the theory To conclude the discussion of Fig. 4, we point out that the picture does not receive substantial modifications if the light fermion χ_0 is not introduced in the theory, and the only NP fermion sits at $m_{\chi_1} = 2.5 \text{ GeV}$. In this case, the $B \rightarrow K + \text{inv.}$ bound does not apply. However, all points with mass $m_V < M_B - M_K$ become subject to the strong resonant $B \rightarrow K^* \mu \mu$ limit, which cuts drastically the parameter space and induces solutions not dissimilar to the area delimited in green in Fig. 4.

Constraints from B_s mixing The parameter space shown in Fig. 4 has not been subject to constraints from B_s mixing, which predominantly proceeds via box diagrams involving dark fermions and heavy coloured scalars, and which in principle could put a strong limit on the NP Yukawa couplings. On the other hand, the LFUV and angular observables in the fit depend only indirectly on y_b and y_s , via the effective coupling \tilde{g} . In the presence of several light fermions, a possible way of suppressing B_s mixing in the limit $m_{\chi_i}/m_\Phi \ll 1$ is obtained when $\sum_{ij} y_s^{i*} y_b^i y_s^{j*} y_b^j \ll 1$, even if one of the χ_i is relatively heavier than the others, as shown in Sec. 3.1.

We illustrate in Fig. 5 the dependence of the B_s -mixing bound, which can limit the size of g_{Vbs} , on the mass of one additional light fermion introduced in the theory as a means to cancelling the $B_s - B_s$ box diagram. We start by plotting g_{Vbs} as a function of the V width, or rather the parameter γ_V^D defined in Eq (2.13). Green points correspond to the solutions also marked in green in Fig. 4, which provide a satisfying fit to the flavour observables and escape $B \rightarrow K + \text{inv.}$ limits when this channel is open. Yellow points show the corresponding case with only χ_1 in the spectrum, which are subject predominantly to the bound from $B \rightarrow K^* \mu \mu$. The parameter space is partially tilted towards the small width for the green points, since the channel $B \rightarrow K + \text{inv.}$ is open and constrain the larger invisible widths.

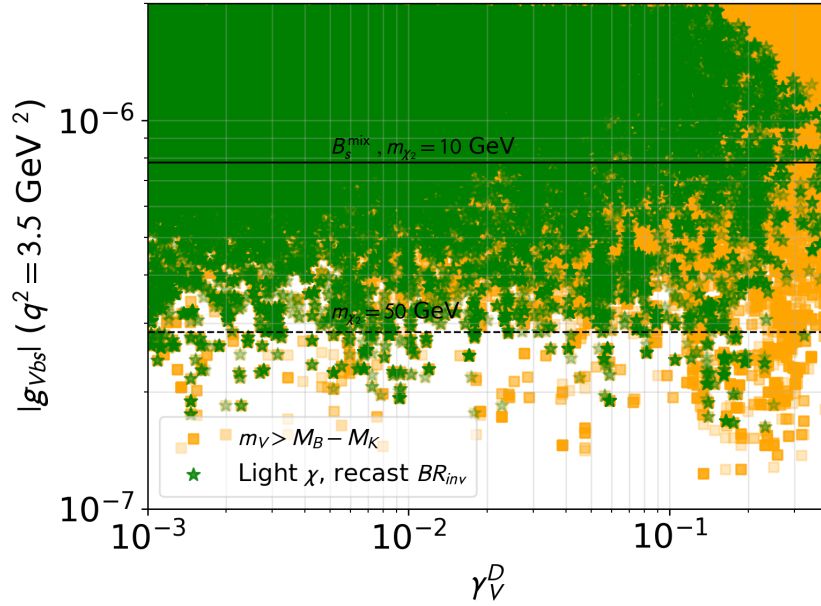


Figure 5: Results of the scan in the high-mass region, $m_V = 2 - 15$ GeV, in the plane of the effective coupling $|g_{Vbs}|$ at $q^2 = 3.5$ GeV² versus γ_V^D . All points in the plot satisfy the flavour constraints at 2σ . Yellow squares have $m_V > M_B - M_K$ by default, while green stars lie on a broader mass range but must survive the $B \rightarrow K + \text{inv.}$ limit. The latter is obtained from our recasting procedure assuming V has a $\sim 100\%$ decay rate into a light dark fermion with $m_{\chi_0} \ll (M_B - M_K)/2$. Horizontal grey lines represent the upper bound from B_s mixing on the effective coupling, under the assumption $y_s^{1*}y_b^1 + y_s^{2*}y_b^2 = 0$ for two different mass values of the compensating dark fermion: $m_{\chi_2} = 10$ GeV (solid) and $m_{\chi_2} = 50$ GeV (dashed).

The presence or not of the light state χ_0 has little influence on the overall B_s -mixing constraints due to its small Yukawa couplings. On the other hand, the box-diagram induced contribution from χ_1 would limit g_{Vbs} to be around 10^{-8} , indicating the need for an additional contribution to B_s -mixing in the UV of the theory. As we have discussed previously in Sec. 3.1, a particularly simple way out invokes the presence of an extra, more massive, dark fermion χ_2 . The solid line shows the upper bound on g_{Vbs} when $m_{\chi_2} = 10$ GeV, $g_D = \sqrt{4\pi}$, and we impose $\delta_Y = y_s^{1*}y_b^1 + y_s^{2*}y_b^2 = 0$. The corresponding limit when $m_{\chi_2} = 50$ GeV is shown with a dashed line. Reducing the fine tuning to $\delta_Y = 0.05$ lowers the lines by a factor of 5.

Results for low-mass We show in Fig. 6 the results of the scan for the low-mass range, $m_V = 0.6 - 2$ GeV, in the (m_V, g_μ^V) plane. Recall that to obtain this region of the parameter space one has to switch the sign in the product $r \cdot g_\mu^V$ with respect to the high-mass region. The procedure allows one to fit $R_{K^{(*)}}$ correctly by means of destructive interference with the SM value of C_9^μ below the experimental bin. The colour code in Fig. 6 is the same as in Fig. 4. Note that in this region the mediator *must have* a sizeable invisible width to

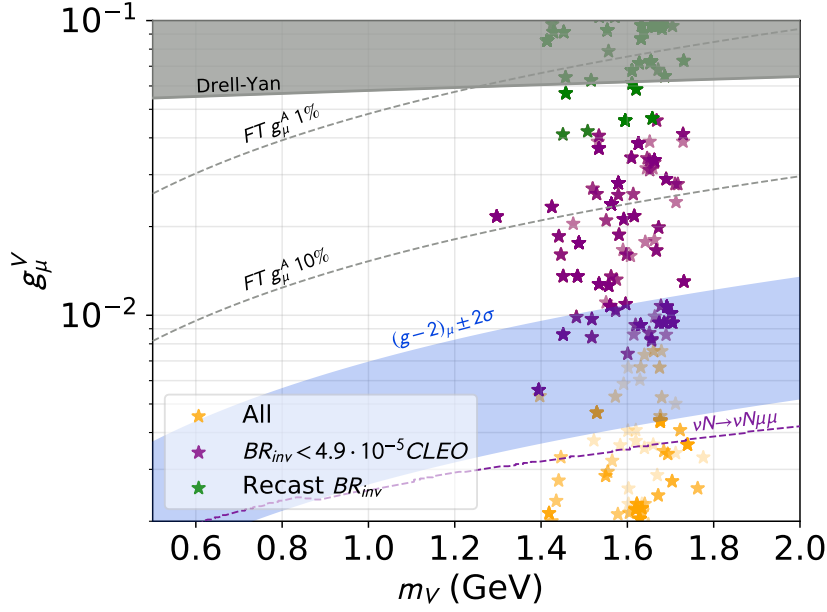


Figure 6: Results of the scan in the low m_V region. The colour code is the same as in Fig. 4.

avoid stringent constraints from a visible dimuon resonance in the $B \rightarrow K^*$ spectrum, as discussed in Sec. 3.1. The presence of at least one light fermion χ_0 besides χ_1 is therefore given for granted.

A few takeaways emerge from the scan in the low-mass region. The first is that there are no solutions with mass $m_V \lesssim 1.4$ GeV. In fact, they are cut out by the $\mathcal{BR}(B_s \rightarrow \mu\mu)$ constraint, which is directly implemented in the likelihood function. Besides the mass cut, the surviving points are all characterised by fairly large values of $R_{K^{(*)}}$, which both lie $2 - 3\sigma$ away from the central value measured at LHCb and closer to their SM expectation. For the same reason, the plot appears much sparser than in the high-mass case: very few model points can be found within 2σ of the measured values of LFUV observables and $\mathcal{BR}(B_s \rightarrow \mu\mu)$ simultaneously. We thus identify a mild tension in this part of the parameter space.

Note also that the models surviving the bound from $B \rightarrow K + \text{inv.}$ searches (green points) require a large coupling g_μ^V to the muon, as \tilde{g} is directly constrained by the invisible search. This means a large level of fine tuning in the corresponding g_μ^A value necessary to cancel $\delta(g - 2)_\mu$. Overall, it is clear that the low-mass region is under siege from a combination of complementary bounds but at present it is not entirely excluded.

Let us finish this section by mentioning the case of a very light mediator: a new gauge boson with mass in the MeV range while dark fermions lie in the GeV scale. An interesting property of this regime is that, in the limit where $2m_{\chi_i} > M_B - M_K$, the mediator V is essentially long-lived since it does not have any available tree-level decay channel. The invisible B decay is then driven exclusively by the $B \rightarrow KV$ process, which is

strongly suppressed at low m_V . Furthermore, the dependence of the Wilson coefficients on $q^2/(q^2 - m_V^2)$ converges to a constant when $m_V \ll q$ and it closely resembles the standard electromagnetic penguin contribution to the flavour anomalies. However, given that the limit from $B_s \rightarrow \mu\mu$ decay forbids such a light vector mediator to have a significant axial-vector coupling to the muon, cf. Eqs. (3.3), (3.4), one cannot avoid the upper bound on the vector coupling arising from $\delta(g - 2)_\mu$: $g_\mu^V \lesssim 7 \times 10^{-4}$. Concretely, in order to obtain $C_9^\mu \approx -0.7$ a coupling $\tilde{g} \gtrsim 10^{-6} \text{ GeV}^{-2}$ is required, which can only be achieved while satisfying $B \rightarrow K + \text{inv.}$ limits if $m_V \lesssim 5 \text{ MeV}$, cf. Fig. 3. A vector mediator this light is already excluded by the standard searches for long-lived dark photon. We conclude that no solution with V in the MeV range is available in penguin-generated scenarios.

Dark matter As an interesting aside, the lightest dark fermion can provide a good example of *forbidden dark matter* candidate when its mass is below the muon mass. The dominant annihilation channel for such a dark matter candidate would be $\chi_0 \bar{\chi}_0 \rightarrow V^* \rightarrow \mu \bar{\mu}$. Such a process leads to a typical relic density of

$$\Omega h^2 \approx 0.05 \left(\frac{100 \text{ MeV}}{m_{\chi_0}} \right)^2 \left(\frac{m_V}{8 \text{ GeV}} \right)^4 \left(\frac{0.05}{g_\mu^V} \right)^2 \left(\frac{1}{\alpha_D} \right) e^{-2\Delta \cdot x_f}, \quad (4.1)$$

where $x_f \approx 20$ for the relevant masses, $g_D = \sqrt{4\pi}$ and $\Delta = 1 - m_{\chi_0}/M_\mu$.

When m_{χ_0} drops below the muon mass threshold the relic density is exponentially enhanced since the annihilation process can only occur due to the thermal velocity of the dark matter particle in the early universe [88, 89]. This ensures that the thermal target is matched for one coupling-dependent mass below M_μ , typically around $\sim M_\mu/2$. Furthermore, all other annihilation processes are exponentially suppressed when the universe temperature decreases, ensuring that the CMB limits on late-time annihilating sub-GeV dark matter are automatically escaped.

5 Conclusions

We have presented in this work a solution for the $b \rightarrow s$ flavour anomalies based on the presence of a split dark sector with a light vector mediator as well as new light Dirac fermions which may constitute all or part of the dark matter. The interaction with the b and s quarks is generated at the loop level via the addition of a coloured scalar particle, resembling a supersymmetric squark. We analysed numerically and analytically the resulting low-energy effective theory, which in particular possesses a q^2 -dependent interaction of the vector mediator with b and s quarks. Varying the mass of the vector mediator from the MeV scale to the tens of GeV, we find two scenarios satisfying all experimental constraints while providing a good fit to the anomalies. In particular, the region with a GeV-scale mediator above the $B - K$ mass threshold appears particularly promising, requiring little to no tuning in the low-energy effective parameters, and to the best of our knowledge it has not been considered previously.

Since our model is partially embedded in a UV completion, we have additionally pointed out several constraints that can challenge its viability. We have highlighted the

constraints from the $B \rightarrow K + \text{inv.}$ decay rate and B_s mixing and, in the latter case, provided an example of a mechanism to escape it. We did not make any assumption in this paper on the nature of the dark Dirac-fermion interactions with the neutrinos. Indeed, since the former are complete SM singlets, it would be very interesting to investigate whether or not they could behave as right-handed neutrinos (for instance via the coupling to a dark charged new Higgs doublet), and in that case investigate their relationship with the strong neutrino trident limits.

While the experimental constraints on models addressing the flavour anomalies with light mediators are already quite stringent, we have identified several observables that can easily exclude these scenarios entirely or provide smoking-gun proof of their detection. Chief among those are the limits from $B \rightarrow K$ and $B \rightarrow K^*$ transitions. While the former play a critical role via the $B \rightarrow K + \text{inv.}$ bounds, experimental searches are typically optimised for the SM process $B \rightarrow K\nu\nu$. Including an analysis based on a light, and potentially broad, invisible resonance $B \rightarrow KV$ could likely strengthen significantly the existing limits, especially when the mediator is light. Similarly, the latest search for $B \rightarrow K^*\mu\mu$ has focused on a very narrow resonance, and should be properly recast for the case of a large and invisible width. Finally, it is important to note that limits on a light dark photon are due to improve in the next few years, and will further constrain the case of a mediator at and below the GeV scale.

Acknowledgments

LD thanks S. Robertson, M. Heck, M. Williams and G. De Pietro for interesting discussions. We thank Pere Arnau for pointing out a factor of 2 mistake in the normalisation of Eq. (2.8). LD is supported by the INFN “Iniziativa Specifica” Theoretical Astroparticle Physics (TAsP-LNF). MF is supported by the MINECO grant FPA2016-76005-C2-1-P and by Maria de Maetzu program grant MDM-2014-0367 of ICCUB and 2017 SGR 929. KK is supported in part by the National Science Centre (Poland) under the research Grant No. 2017/26/E/ST2/00470. EMS is supported in part by the National Science Centre (Poland) under the research Grant No. 2017/26/D/ST2/00490.

A Appendix: Invisible decay limits

We present in this appendix a more detailed treatment of the recasting procedure performed to extract conservative $B \rightarrow K + \text{inv.}$ limits on our model.

While the CLEO Collaboration searched explicitly for an on-shell light particle mediating the $B \rightarrow K$ decay [87], their 2σ limit $\mathcal{BR}(B \rightarrow K + \text{inv.}) < 4.9 \times 10^{-5}$ is relatively weak compared to the ones from B factories. In the following we will base our limit both on the BaBar result [68] – which provides a differential branching ratio limit in bins of q^2 – as well as on an older analysis from the same collaboration [69], which also had some differential limits, albeit on a much larger range for q^2 . Note that the current bounds from the Belle Collaboration [70, 71] are typically of the same order as for BaBar. They are however strongly optimised for the SM-like $B \rightarrow K\nu\nu$ signal and only present their bounds in the total integrated branching ratio. We therefore concentrate on the two BaBar analyses.

First, using the BaBar hadronic-tagging analysis [68], we calculate the branching ratio $\mathcal{BR}(B \rightarrow K\chi_1\chi_1)$ in $s_B = q^2/M_B^2$ bins, where for low m_V most of our NP signal is concentrated in the lowest bin, $s_B < 0.1$. We then compare it with the 2σ limits from Fig. 6a of ref. [68]. While this approach leads to a strong bound when the real process $B \rightarrow KV$, $V \rightarrow \chi_0\chi_0$ dominates, these limits can be significantly weakened when the virtual process dominates, since the branching ratio accounts for a broader spread in s_B bins.

We therefore also include partially integrated limits from the BaBar semileptonic-tagging analysis [69], which combined the world-leading limit on $B^+ \rightarrow K^+\nu\nu$ with detailed information about the signal efficiencies as function of the momentum of the K^+ (and hence on the missing energy). We select the q^2 ranges $[3.4^2, 4^2] \text{ GeV}^2$ and $[0, 2.4^2] \text{ GeV}^2$ (corresponding to p_K in the range $[1, 1.5] \text{ GeV}$ and $\gtrsim 2 \text{ GeV}$, respectively), where the Boosted Decision Tree (BDT) efficiencies presented in Fig. 3 of ref. [69] are larger than ~ 0.3 . This ensures that the signal efficiencies for our NP kinematics are of the same order of magnitude or higher than the ones for the SM signal. We then compare both regions with the low- q^2 and high- q^2 95% C.L. limits, $\mathcal{BR}(B \rightarrow K + \text{inv.}) < 1.1 \times 10^{-5}$ and $\mathcal{BR}(B \rightarrow K + \text{inv.}) < 4.6 \times 10^{-5}$, respectively.

References

- [1] **LHCb** Collaboration, R. Aaij et al., *Test of lepton universality using $B^+ \rightarrow K^+\ell^+\ell^-$ decays*, *Phys. Rev. Lett.* **113** (2014) 151601, [[arXiv:1406.6482](#)].
- [2] **LHCb** Collaboration, R. Aaij et al., *Test of lepton universality with $B^0 \rightarrow K^{*0}\ell^+\ell^-$ decays*, *JHEP* **08** (2017) 055, [[arXiv:1705.05802](#)].
- [3] **LHCb** Collaboration, R. Aaij et al., *Search for lepton-universality violation in $B^+ \rightarrow K^+\ell^+\ell^-$ decays*, [[arXiv:1903.09252](#)].
- [4] **Belle** Collaboration, A. Abdesselam et al., *Test of lepton flavor universality in $B \rightarrow K^*\ell^+\ell^-$ decays at Belle*, [[arXiv:1904.02440](#)].

- [5] **LHCb** Collaboration, R. Aaij et al., *Angular analysis of the $B^0 \rightarrow K^{*0}\mu^+\mu^-$ decay using 3 fb^{-1} of integrated luminosity*, *JHEP* **02** (2016) 104, [[arXiv:1512.04442](#)].
- [6] **Belle** Collaboration, S. Wehle et al., *Lepton-Flavor-Dependent Angular Analysis of $B \rightarrow K^*\ell^+\ell^-$* , *Phys. Rev. Lett.* **118** (2017), no. 11 111801, [[arXiv:1612.05014](#)].
- [7] **CMS** Collaboration, A. M. Sirunyan et al., *Measurement of angular parameters from the decay $B^0 \rightarrow K^{*0}\mu^+\mu^-$ in proton-proton collisions at $\sqrt{s} = 8\text{ TeV}$* , *Phys. Lett.* **B781** (2018) 517–541, [[arXiv:1710.02846](#)].
- [8] **ATLAS** Collaboration, M. Aaboud et al., *Angular analysis of $B_d^0 \rightarrow K^*\mu^+\mu^-$ decays in pp collisions at $\sqrt{s} = 8\text{ TeV}$ with the ATLAS detector*, *JHEP* **10** (2018) 047, [[arXiv:1805.04000](#)].
- [9] **LHCb** Collaboration, R. Aaij et al., *Angular analysis and differential branching fraction of the decay $B_s^0 \rightarrow \phi\mu^+\mu^-$* , *JHEP* **09** (2015) 179, [[arXiv:1506.08777](#)].
- [10] **LHCb** Collaboration, R. Aaij et al., *Differential branching fractions and isospin asymmetries of $B \rightarrow K^{(*)}\mu^+\mu^-$ decays*, *JHEP* **06** (2014) 133, [[arXiv:1403.8044](#)].
- [11] **LHCb** Collaboration, R. Aaij et al., *Measurements of the S -wave fraction in $B^0 \rightarrow K^+\pi^-\mu^+\mu^-$ decays and the $B^0 \rightarrow K^*(892)^0\mu^+\mu^-$ differential branching fraction*, *JHEP* **11** (2016) 047, [[arXiv:1606.04731](#)]. [Erratum: *JHEP*04,142(2017)].
- [12] W. Altmannshofer and D. M. Straub, *New physics in $b \rightarrow s$ transitions after LHC run 1*, *Eur. Phys. J.* **C75** (2015), no. 8 382, [[arXiv:1411.3161](#)].
- [13] W. Altmannshofer, C. Niehoff, P. Stangl, and D. M. Straub, *Status of the $B \rightarrow K^*\mu^+\mu^-$ anomaly after Moriond 2017*, *Eur. Phys. J.* **C77** (2017), no. 6 377, [[arXiv:1703.09189](#)].
- [14] B. Capdevila, A. Crivellin, S. Descotes-Genon, J. Matias, and J. Virto, *Patterns of New Physics in $b \rightarrow s\ell^+\ell^-$ transitions in the light of recent data*, *JHEP* **01** (2018) 093, [[arXiv:1704.05340](#)].
- [15] W. Altmannshofer, P. Stangl, and D. M. Straub, *Interpreting Hints for Lepton Flavor Universality Violation*, *Phys. Rev.* **D96** (2017), no. 5 055008, [[arXiv:1704.05435](#)].
- [16] G. D’Amico, M. Nardecchia, P. Panci, F. Sannino, A. Strumia, R. Torre, and A. Urbano, *Flavour anomalies after the R_{K^*} measurement*, *JHEP* **09** (2017) 010, [[arXiv:1704.05438](#)].
- [17] M. Ciuchini, A. M. Coutinho, M. Fedele, E. Franco, A. Paul, L. Silvestrini, and M. Valli, *On Flavourful Easter eggs for New Physics hunger and Lepton Flavour Universality violation*, *Eur. Phys. J.* **C77** (2017), no. 10 688, [[arXiv:1704.05447](#)].
- [18] A. K. Alok, B. Bhattacharya, A. Datta, D. Kumar, J. Kumar, and D. London, *New Physics in $b \rightarrow s\mu^+\mu^-$ after the Measurement of R_{K^*}* , *Phys. Rev.* **D96** (2017), no. 9 095009, [[arXiv:1704.07397](#)].
- [19] T. Hurth, F. Mahmoudi, and S. Neshatpour, *Global fits to $b \rightarrow s\ell\ell$ data and signs for lepton non-universality*, *JHEP* **12** (2014) 053, [[arXiv:1410.4545](#)].
- [20] T. Hurth, F. Mahmoudi, and S. Neshatpour, *On the anomalies in the latest LHCb data*, *Nucl. Phys.* **B909** (2016) 737–777, [[arXiv:1603.00865](#)].
- [21] V. G. Chobanova, T. Hurth, F. Mahmoudi, D. Martinez Santos, and S. Neshatpour, *Large hadronic power corrections or new physics in the rare decay $B \rightarrow K^*\mu^+\mu^-$?*, *JHEP* **07** (2017) 025, [[arXiv:1702.02234](#)].

- [22] T. Hurth, F. Mahmoudi, D. Martinez Santos, and S. Neshatpour, *Lepton nonuniversality in exclusive $b \rightarrow s \ell \ell$ decays*, *Phys. Rev.* **D96** (2017), no. 9 095034, [[arXiv:1705.06274](#)].
- [23] A. Arbey, T. Hurth, F. Mahmoudi, and S. Neshatpour, *Hadronic and New Physics Contributions to $b \rightarrow s$ Transitions*, *Phys. Rev.* **D98** (2018), no. 9 095027, [[arXiv:1806.02791](#)].
- [24] M. Algueró, B. Capdevila, A. Crivellin, S. Descotes-Genon, P. Masjuan, J. Matias, and J. Virto, *Emerging patterns of New Physics with and without Lepton Flavour Universal contributions*, *Eur. Phys. J.* **C79** (2019), no. 8 714, [[arXiv:1903.09578](#)].
- [25] A. K. Alok, A. Dighe, S. Gangal, and D. Kumar, *Continuing search for new physics in $b \rightarrow s \mu \mu$ decays: two operators at a time*, *JHEP* **06** (2019) 089, [[arXiv:1903.09617](#)].
- [26] M. Ciuchini, A. M. Coutinho, M. Fedele, E. Franco, A. Paul, L. Silvestrini, and M. Valli, *New Physics in $b \rightarrow s \ell^+ \ell^-$ confronts new data on Lepton Universality*, *Eur. Phys. J.* **C79** (2019), no. 8 719, [[arXiv:1903.09632](#)].
- [27] A. Datta, J. Kumar, and D. London, *The B anomalies and new physics in $b \rightarrow s e^+ e^-$* , *Phys. Lett.* **B797** (2019) 134858, [[arXiv:1903.10086](#)].
- [28] J. Aebischer, W. Altmannshofer, D. Guadagnoli, M. Reboud, P. Stangl, and D. M. Straub, *B -decay discrepancies after Moriond 2019*, [arXiv:1903.10434](#).
- [29] K. Kowalska, D. Kumar, and E. M. Sessolo, *Implications for new physics in $b \rightarrow s \mu \mu$ transitions after recent measurements by Belle and LHCb*, *Eur. Phys. J.* **C79** (2019), no. 10 840, [[arXiv:1903.10932](#)].
- [30] A. Arbey, T. Hurth, F. Mahmoudi, D. M. Santos, and S. Neshatpour, *Update on the $b \rightarrow s$ anomalies*, *Phys. Rev.* **D100** (2019), no. 1 015045, [[arXiv:1904.08399](#)].
- [31] S. Bhattacharya, A. Biswas, S. Nandi, and S. K. Patra, *Exhaustive Model Selection in $b \rightarrow s \ell \ell$ Decays: Pitting Cross-Validation against AIC_c* , [arXiv:1908.04835](#).
- [32] A. Datta, J. Liao, and D. Marfatia, *A light Z' for the R_K puzzle and nonstandard neutrino interactions*, *Phys. Lett.* **B768** (2017) 265–269, [[arXiv:1702.01099](#)].
- [33] F. Sala and D. M. Straub, *A New Light Particle in B Decays?*, *Phys. Lett.* **B774** (2017) 205–209, [[arXiv:1704.06188](#)].
- [34] A. Datta, J. Kumar, J. Liao, and D. Marfatia, *New light mediators for the R_K and R_{K^*} puzzles*, *Phys. Rev.* **D97** (2018), no. 11 115038, [[arXiv:1705.08423](#)].
- [35] W. Altmannshofer, M. J. Baker, S. Gori, R. Harnik, M. Pospelov, E. Stamou, and A. Thamm, *Light resonances and the low- q^2 bin of R_{K^*}* , *JHEP* **03** (2018) 188, [[arXiv:1711.07494](#)].
- [36] A. Datta, J. L. Feng, S. Kamali, and J. Kumar, *Resolving the $(g-2)_\mu$ and B Anomalies with Leptoquarks and a Dark Higgs Boson*, *Phys. Rev.* **D101** (2020), no. 3 035010, [[arXiv:1908.08625](#)].
- [37] J. Lyon and R. Zwicky, *Resonances gone topsy turvy - the charm of QCD or new physics in $b \rightarrow s \ell^+ \ell^-$?*, [arXiv:1406.0566](#).
- [38] LHCb Collaboration, R. Aaij et al., *Angular analysis of the $B^0 \rightarrow K^{*0} e^+ e^-$ decay in the low- q^2 region*, *JHEP* **04** (2015) 064, [[arXiv:1501.03038](#)].
- [39] B. Gripaios, M. Nardecchia, and S. A. Renner, *Linear flavour violation and anomalies in B physics*, *JHEP* **06** (2016) 083, [[arXiv:1509.05020](#)].

- [40] P. Arnan, L. Hofer, F. Mescia, and A. Crivellin, *Loop effects of heavy new scalars and fermions in $b \rightarrow s\mu^+\mu^-$* , *JHEP* **04** (2017) 043, [[arXiv:1608.07832](#)].
- [41] J. M. Cline and J. M. Cornell, *$R(K^{(*)})$ from dark matter exchange*, *Phys. Lett.* **B782** (2018) 232–237, [[arXiv:1711.10770](#)].
- [42] A. Crivellin, C. Greub, D. Müller, and F. Saturnino, *Importance of Loop Effects in Explaining the Accumulated Evidence for New Physics in B Decays with a Vector Leptoquark*, *Phys. Rev. Lett.* **122** (2019), no. 1 011805, [[arXiv:1807.02068](#)].
- [43] A. Datta, B. Dutta, S. Liao, D. Marfatia, and L. E. Strigari, *Neutrino scattering and B anomalies from hidden sector portals*, *JHEP* **01** (2019) 091, [[arXiv:1808.02611](#)].
- [44] B. Barman, D. Borah, L. Mukherjee, and S. Nandi, *Correlating the anomalous results in $b \rightarrow s$ decays with inert Higgs doublet dark matter and muon $(g-2)$* , *Phys. Rev.* **D100** (2019), no. 11 115010, [[arXiv:1808.06639](#)].
- [45] C. Marzo, L. Marzola, and M. Raidal, *Common explanation to the $R_{K^{(*)}}$, $R_{D^{(*)}}$ and ϵ'/ϵ anomalies in a $3\text{HDM}+\nu_R$ and connections to neutrino physics*, *Phys. Rev.* **D100** (2019), no. 5 055031, [[arXiv:1901.08290](#)].
- [46] P. Arnan, A. Crivellin, M. Fedele, and F. Mescia, *Generic loop effects of new scalars and fermions in $b \rightarrow s\ell^+\ell^-$ and a vector-like 4th generation*, *JHEP* **06** (2019) 118, [[arXiv:1904.05890](#)].
- [47] J. Kawamura, S. Okawa, and Y. Omura, *Interplay between the $b \rightarrow s\ell\ell$ anomalies and dark matter physics*, *Phys. Rev.* **D96** (2017), no. 7 075041, [[arXiv:1706.04344](#)].
- [48] **ATLAS** Collaboration, M. Aaboud et al., *Search for supersymmetry in events with b -tagged jets and missing transverse momentum in pp collisions at $\sqrt{s} = 13$ TeV with the ATLAS detector*, *JHEP* **11** (2017) 195, [[arXiv:1708.09266](#)].
- [49] **ATLAS** Collaboration, M. Aaboud et al., *Search for a scalar partner of the top quark in the jets plus missing transverse momentum final state at $\sqrt{s}=13$ TeV with the ATLAS detector*, *JHEP* **12** (2017) 085, [[arXiv:1709.04183](#)].
- [50] **CMS** Collaboration, A. M. Sirunyan et al., *Search for direct top squark pair production in events with one lepton, jets, and missing transverse momentum at 13 TeV with the CMS experiment*, [arXiv:1912.08887](#).
- [51] **CMS** Collaboration, A. M. Sirunyan et al., *Search for supersymmetry in proton-proton collisions at 13 TeV in final states with jets and missing transverse momentum*, *JHEP* **10** (2019) 244, [[arXiv:1908.04722](#)].
- [52] L. Di Luzio, M. Kirk, and A. Lenz, *Updated B_s -mixing constraints on new physics models for $b \rightarrow s\ell^+\ell^-$ anomalies*, *Phys. Rev.* **D97** (2018), no. 9 095035, [[arXiv:1712.06572](#)].
- [53] K. Kowalska and E. M. Sessolo, *Expectations for the muon $g-2$ in simplified models with dark matter*, *JHEP* **09** (2017) 112, [[arXiv:1707.00753](#)].
- [54] **CMS** Collaboration, A. M. Sirunyan et al., *Searches for pair production of charginos and top squarks in final states with two oppositely charged leptons in proton-proton collisions at $\sqrt{s} = 13$ TeV*, *JHEP* **11** (2018) 079, [[arXiv:1807.07799](#)].
- [55] **ATLAS** Collaboration, G. Aad et al., *Search for electroweak production of charginos and sleptons decaying into final states with two leptons and missing transverse momentum in $\sqrt{s} = 13$ TeV pp collisions using the ATLAS detector*, *Eur. Phys. J.* **C80** (2020), no. 2 123, [[arXiv:1908.08215](#)].

- [56] **Muon g-2** Collaboration, G. W. Bennett et al., *Final Report of the Muon E821 Anomalous Magnetic Moment Measurement at BNL*, *Phys. Rev.* **D73** (2006) 072003, [[hep-ex/0602035](#)].
- [57] M. Davier, *Update of the Hadronic Vacuum Polarisation Contribution to the muon g-2*, *Nucl. Part. Phys. Proc.* **287-288** (2017) 70–75, [[arXiv:1612.02743](#)].
- [58] F. Jegerlehner, *Muon g-2 theory: The hadronic part*, *EPJ Web Conf.* **166** (2018) 00022, [[arXiv:1705.00263](#)].
- [59] W. Altmannshofer, S. Gori, M. Pospelov, and I. Yavin, *Neutrino Trident Production: A Powerful Probe of New Physics with Neutrino Beams*, *Phys. Rev. Lett.* **113** (2014) 091801, [[arXiv:1406.2332](#)].
- [60] **CCFR** Collaboration, S. R. Mishra et al., *Neutrino tridents and W Z interference*, *Phys. Rev. Lett.* **66** (1991) 3117–3120.
- [61] **CHARM-II** Collaboration, D. Geiregat et al., *First observation of neutrino trident production*, *Phys. Lett.* **B245** (1990) 271–275.
- [62] P. Ko, Y. Omura, and C. Yu, *Higgs phenomenology in type-i 2hdm with u(1)_h higgs gauge symmetry*, *JHEP* **01** (2014) 016, [[arXiv:1309.7156](#)].
- [63] J. Gracey, *Three loop \overline{MS} tensor current anomalous dimension in QCD*, *Phys. Lett. B* **488** (2000) 175–181, [[hep-ph/0007171](#)].
- [64] **CMS** Collaboration, S. Chatrchyan et al., *Measurement of the $b^0 \rightarrow \mu^+ \mu^-$ branching fraction and search for $b^0 \rightarrow \mu^+ \mu^-$ with the cms experiment*, *Phys.Rev.Lett.* **111** (2013) 101804, [[arXiv:1307.5025](#)].
- [65] **CMS, LHCb** Collaboration, V. Khachatryan et al., *Observation of the rare $b^0 \rightarrow \mu^+ \mu^-$ decay from the combined analysis of cms and lhcb data*, *Nature* **522** (2015) 68–72, [[arXiv:1411.4413](#)].
- [66] **LHCb** Collaboration, R. Aaij et al., *Measurement of the $b^0 \rightarrow \mu^+ \mu^-$ branching fraction and effective lifetime and search for $b^0 \rightarrow \mu^+ \mu^-$ decays*, *Phys.Rev.Lett.* **118** (2017), no. 19 191801, [[arXiv:1703.05747](#)].
- [67] **ATLAS** Collaboration, M. Aaboud et al., *Study of the rare decays of $b^0 \rightarrow \mu^+ \mu^-$ and b^0 mesons into muon pairs using data collected during 2015 and 2016 with the atlas detector*, *JHEP* **04** (2019) 098, [[arXiv:1812.03017](#)].
- [68] **BaBar** Collaboration, J. P. Lees et al., *Search for $B \rightarrow K^{(*)} \nu \bar{\nu}$ and invisible quarkonium decays*, *Phys. Rev.* **D87** (2013), no. 11 112005, [[arXiv:1303.7465](#)].
- [69] **BaBar** Collaboration, P. del Amo Sanchez et al., *Search for the Rare Decay $B \rightarrow K \nu \bar{\nu}$* , *Phys. Rev.* **D82** (2010) 112002, [[arXiv:1009.1529](#)].
- [70] **Belle** Collaboration, O. Lutz et al., *Search for $B \rightarrow h^{(*)} \nu \bar{\nu}$ with the full Belle $\Upsilon(4S)$ data sample*, *Phys. Rev.* **D87** (2013), no. 11 111103, [[arXiv:1303.3719](#)].
- [71] **Belle** Collaboration, J. Grygier et al., *Search for $B \rightarrow h \nu \bar{\nu}$ decays with semileptonic tagging at Belle*, *Phys. Rev.* **D96** (2017), no. 9 091101, [[arXiv:1702.03224](#)]. [Addendum: *Phys. Rev.* **D97**, no. 9, 099902 (2018)].
- [72] **LHCb** Collaboration, R. Aaij et al., *Search for hidden-sector bosons in $B^0 \rightarrow K^{*0} \mu^+ \mu^-$ decays*, *Phys. Rev. Lett.* **115** (2015), no. 16 161802, [[arXiv:1508.04094](#)].
- [73] T. R. Slatyer, *Indirect dark matter signatures in the cosmic dark ages. I. Generalizing the*

- bound on s -wave dark matter annihilation from Planck results, *Phys. Rev.* **D93** (2016), no. 2 023527, [[arXiv:1506.03811](#)].
- [74] J. A. Bailey et al., $B \rightarrow Kl^+l^-$ Decay Form Factors from Three-Flavor Lattice QCD, *Phys. Rev.* **D93** (2016), no. 2 025026, [[arXiv:1509.06235](#)].
- [75] F. Jegerlehner and A. Nyffeler, *The Muon $g-2$* , *Phys. Rept.* **477** (2009) 1–110, [[arXiv:0902.3360](#)].
- [76] F. S. Queiroz and W. Shepherd, *New Physics Contributions to the Muon Anomalous Magnetic Moment: A Numerical Code*, *Phys. Rev.* **D89** (2014), no. 9 095024, [[arXiv:1403.2309](#)].
- [77] W. Altmannshofer, S. Gori, M. Pospelov, and I. Yavin, *Quark flavor transitions in $L_\mu - L_\tau$ models*, *Phys. Rev.* **D89** (2014) 095033, [[arXiv:1403.1269](#)].
- [78] **ALEPH, DELPHI, L3, OPAL, SLD, LEP Electroweak Working Group, SLD Electroweak Group, SLD Heavy Flavour Group** Collaboration, S. Schael et al., *Precision electroweak measurements on the Z resonance*, *Phys. Rept.* **427** (2006) 257–454, [[hep-ex/0509008](#)].
- [79] F. Bishara, U. Haisch, and P. F. Monni, *Regarding light resonance interpretations of the B decay anomalies*, *Phys. Rev.* **D96** (2017), no. 5 055002, [[arXiv:1705.03465](#)].
- [80] **Belle-II** Collaboration, I. Adachi et al., *Search for an Invisibly Decaying Z' Boson at Belle II in $e^+e^- \rightarrow \mu^+\mu^-(e^\pm\mu^\mp)$ Plus Missing Energy Final States*, [arXiv:1912.11276](#).
- [81] L. Darmé, S. A. R. Ellis, and T. You, *Light Dark Sectors through the Fermion Portal*, [arXiv:2001.01490](#).
- [82] J. Beacham et al., *Physics Beyond Colliders at CERN: Beyond the Standard Model Working Group Report*, *J. Phys.* **G47** (2020), no. 1 010501, [[arXiv:1901.09966](#)].
- [83] G. Durieux, F. Maltoni, and C. Zhang, *Global approach to top-quark flavor-changing interactions*, *Phys. Rev.* **D91** (2015), no. 7 074017, [[arXiv:1412.7166](#)].
- [84] M. Chala, J. Santiago, and M. Spannowsky, *Constraining four-fermion operators using rare top decays*, [arXiv:1809.09624](#).
- [85] J. De Blas et al., *HEPfit: a code for the combination of indirect and direct constraints on high energy physics models*, [arXiv:1910.14012](#).
- [86] A. Caldwell, D. Kollar, and K. Kroninger, *BAT: The Bayesian Analysis Toolkit*, *Comput. Phys. Commun.* **180** (2009) 2197–2209, [[arXiv:0808.2552](#)].
- [87] **CLEO** Collaboration, R. Ammar et al., *Search for the familon via $B^\pm \rightarrow \pi^\pm X^0$, $B^\pm \rightarrow K^\pm X^0$, and $B^0 \rightarrow K_S^0 X^0$ decays*, *Phys. Rev. Lett.* **87** (2001) 271801, [[hep-ex/0106038](#)].
- [88] K. Griest and D. Seckel, *Three exceptions in the calculation of relic abundances*, *Phys. Rev.* **D43** (1991) 3191–3203.
- [89] R. T. D’Agnolo and J. T. Ruderman, *Light Dark Matter from Forbidden Channels*, *Phys. Rev. Lett.* **115** (2015), no. 6 061301, [[arXiv:1505.07107](#)].